Songklanakarin J. Sci. Technol.
31 (2), 205-212, Mar. - Apr. 2009

Songklanakarin Journal of Science and Technology
http://rdo.psu.ac.th/sjst

Original Article

Development of Window-based program for analysis and visualization of two-dimensional stress field in digital photoelasticity

Pichet Pinit*

Department of Mechanical Technology Education, Faculty of Industrial Education and Technology
King Mongkut's University of Technology Thonburi, Bangmod, Thung Khru, Bangkok, 10140 Thailand.

Received 20 May 2008; Accepted 5 January 2009

Abstract

This paper describes the development of a Window-based framework for analyzing and visualizing two-dimensional stress field in digital photoelasticity. The program is implemented as stand-alone software. The program contains mainly two parts: computational part and visual part supplemented with several image-processing functions. The computation method used in the program for retrieval of photoelastic parameters (isoclinic and isochromatic parameters) is the phase stepping method. The visualization links between the results and the user by a gray scale or color map of such parameters, which is very convenient to the user for physical interpretation. With the Windows-based framework, additional modules either computation or visualization can be simply added to the program.

Keywords: digital photoelasticity, isochromatic parameter, isoclinic parameter, phase stepping method, phase unwrapping

1. Introduction

Engineering design is of great importance in the engineering field. Problem-solving methods can be classified into three main types: theoretical or analytical method, numerical method, and experimental method. Figure 1 show the diagram of these three methods with some of their elements. Analytical method provides several (exact) solutions for particular engineering problems and these solutions are available from the Theory of Elasticity and/or Theory of Plasticity. Obtaining these kinds of solutions requires, however, great knowledge of mathematics and is considerably rigorous. This limitation brought alive the numerical method (Finite different method, Finite element analysis, etc) when digital computers become available. The numerical method can rapidly solve the problems and provide a neat visualization of data to ease the physical interpretation. These aspects make the numerical method widely used as they are applied to many fields of research other than the engineering design. It should, however, be noted here that in the context of the engineering design any result obtained from the numerical method is meaningless if the governing equations are not derived from, or are inconsistent with, the theory of elasticity or plasticity. The numerical method is, therefore, just a computational tool helping the engineer's works.

In the development of analytical method, other methods are necessary for validation since the analytical method is not presented in the real world because of its

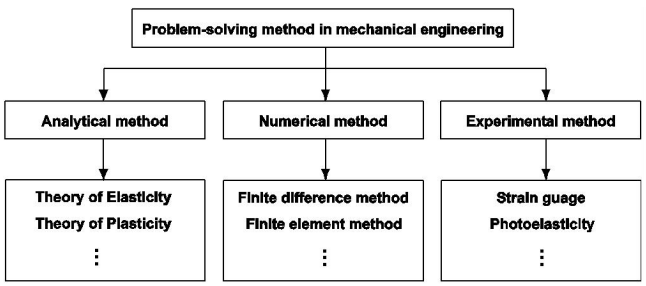

Figure 1. Classification of problem-solving methods in mechanical engineering.

*Corresponding author.
Email address: pichet.pin@kmutt.ac.th

assumptions. However, the real world is the right place for an experimental method. Pindera (2002) expressed the relationship as "no theory - no experiment" and "no experiment - no theory". This statement points out the paramount importance of the experiment. The role of the experimental method is just to do with discovery, characterization, and verification of the analytical method. A good explanation of the role of the experimental method is given by Krishnaswamy (2005). There are several techniques in the experiment such as strain gauge method, photoelasticity, thermoelasticity, etc. Photoelasticity is the only one technique that provides the stress field in a visual way. It can solve both two- and three-dimensional elastic problems. The principle of photoelasticity is based on the birefringent phenomenon occurring in the transparent materials under the application of external loads. In 1956, the popularity of photoelasticity had dropped due to the development of the numerical method, especially the finite element analysis (Patterson, 2002). In 1990, the photoelasticity came back alive in the new form, i.e., digital photoelasticity. Digital photoelasticity is the combination of conventional photoelasticity and some new techniques in data acquisition and data processing technologies and it is known under the name of automated fringe analysis. Its popularity continuously grows with no signs of its stop (Patterson, 2002). As a result, any research activity under the automated fringe analysis is of great importance to the engineering field. The successful applications of digital photoelasticity can be found in the following works as an example. Patterson and Wang (1991) developed the method for full-field automated photoelastic analysis for the loaded bolt. The successful applications of digital photoelasticity going back in time before 1999 can be found in the Chen's book (1999), selected paper on photoelasticity. Chen *et al.* (2002) proposed a cost-effective method for photoelastic measurement the ball screw contact angle. Further, the application of the digital photoelasticity to investigate the dynamic bending stress of a spur gear was proposed by Wang (2003). Zuccarello and Ferrante (2005) used automated photoelasticity to determine the stress intensity factors for biomaterial joints and Spita *et al.* (2006) used digital photoelasticity as a verification tool for validating the results of the optimum gear tooth geometry with minimum fillet obtained using the boundary element method. Further, Jones *et al.* (2008) investigated the slippage in shrink-fit assemblies using digital photoelasticity.

Though digital photoelasticity is successfully applied to the engineering design as mentioned, it is just maturing. The major problems in digital photoelasticity are that there are two field parameters (see section 2.2) which, by principle, interact on each other and the wrapped phases that have to be unwrapped (Ramesh, 2000). The interaction between them causes error in their final results after unwrapping. Some researchers have paid attention to solving these problems.

Focusing on the stress field retrieved from the stress analysis, it is very difficult for the analysts to imagine how the stress field looks like even though they are just computing the stress values for any point in question. A visualizing tool based on the use of the finite element analysis can easily provide a neat picture of the stress field (Zheng *et al.*, 1995, Wunche, 1999, Jeramic′ *et al.*, 2002). Commercial software in the field of the finite element analysis has this visualizing tool. Although the finite element analysis is a powerful technique for stress visualization, several critical parameters come with it, one of which is the boundary conditions (BCs). At the points or regions to which the BCs are applied (also at the reactive points), the different stress fields would be obtained and this is known to be due to the Saint's Venant principle (Frocht, 1948). On the other hand, in digital photoelasticity, this problem is compensated automatically since digital photoelasticity is an experimental method and these reflect the reality.

With the information described above, this paper is to present a user-friendly program for the use in the digitally photoelastic analysis. The program can be used to determine two-dimensional photoelastic parameters (described in the next section). These parameters are essential in photoelastic analysis. For the simulation module, it provides the simulated photoelastic fringes, which can be used to validate the solutions given from the theory of elasticity.

2. Theoretical background of photoelasticity

2.1 Introduction to photoelasticity

Photoelasticity is one of the experimental methods used for analyzing stress field. The principle of photoelasticity depends on the birefringent phenomenon occurring in the transparent materials under the application of external loads. This phenomenon was first discovered by Brewster in 1816 (Patterson, 2002). With digital photoelasticity, the stress field is expressed as an intensity map which can be simply recorded by digital cameras. In digital photoelasticity, various techniques are available for solving the photoelastic parameters and these can be mainly classified as phase shifting, load stepping, three fringe photoelasticity, and Fourier transform approach (Ramesh, 2000). Of these techniques, the phase shifting (PST) is widely used due to its simplicity and accuracy. Therefore, in the program developed here only PST is considered.

2.2 Formulation of photoelastic fringes

Since the stress field is displayed as an intensity map, it must have the intensity equation that governs the formation of such intensity map. The intensity equation depends on the types of polariscope used, i.e., plane polariscope, circular polariscope, and mix-polariscope (Ramesh, 2000). However, in this paper, only the plane polariscope is considered.

The mathematical model of the intensity coming out of the plane polariscope (Figure 2) can be expressed as (Jones and Wang, 2005)

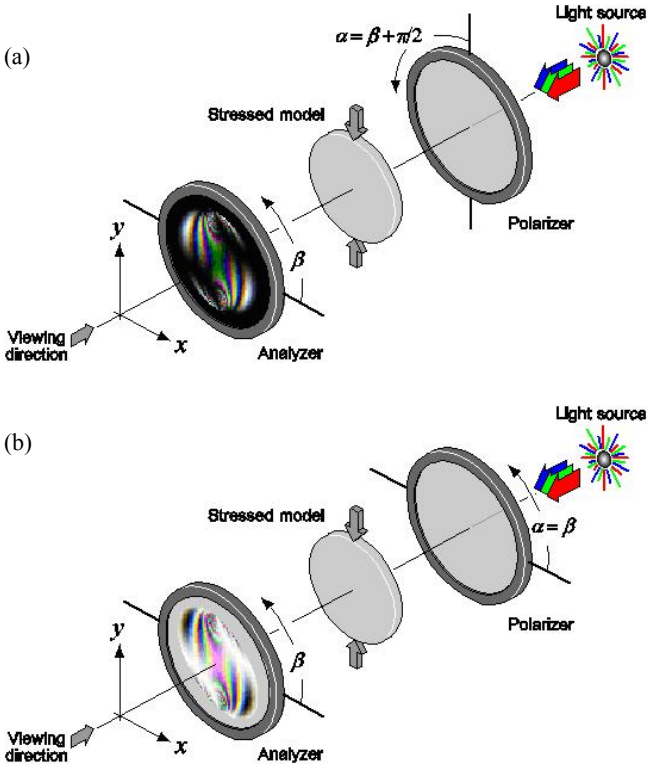

Figure 2. Plane polariscope: (a) dark-field setup and (b) bright-field setup. These images are printed in black and white.

$$I = f(\alpha, \beta, I_p, \phi, N, t, f_\sigma, I_b) \quad (1)$$

where α and β are the optical or polarizing axis of the polarizer and analyzer, respectively, I_p is the intensity coming out of the polarizer, ϕ is the isoclinic angle or the angle between the σ_1 direction and the horizontal axis, N is the fringe order, t is the thickness of the model studied, f_σ is the material stress fringe value (defined later), and I_b is the background intensity.

The relation between the fringe order and the relative retardation, δ, is

$$\delta = 2\pi N = \frac{2\pi t}{\lambda} C(\sigma_1 - \sigma_2) \quad (2)$$

where C is the relative stress-optic coefficient and usually assumed to be a constant for a material and λ is the wavelength used. Eq. (2) can be rewritten as

$$\frac{N f_\sigma}{t} = (\sigma_1 - \sigma_2) \quad (3)$$

where $f_\sigma = \lambda / C$ which can be obtained by a calibration.

Based on the dark-field plane polariscope (Figure 2a), the intensity equation can be written as (Ramesh, 2000)

$$I = I_p \sin^2(\pi N) \sin^2 2(\phi - \beta) + I_b \quad (4)$$

whereas the intensity equation based on the bright-field setup (Figure 2b) is expressed as

$$I = I_p [1 - \sin^2(\pi N) \sin^2 2(\phi - \beta)] + I_b \quad (5)$$

Considering Eq. (4) reveals that the intensity I becomes zero or nearly zero when the fringe order $N = 0, \pm 1, \pm 2, \ldots$ or $\phi = \beta$ or $\beta \pm \pi/2$. The former refers to the isochromatic fringe and the latter refers to the isoclinic fringe. For the isochromatic fringe, the black fringe occurs when such condition is fulfilled whereas for other regions, the fringe appears as color(s) depending on the light source used, i.e., monochromatic light or polychromatic light. For the isoclinic fringe, the black fringe occurs when the polarizing axes of either the polarizer or the analyzer coincide with the directions of σ_1 or σ_2. Since both parameters are continuous over the entire model, both fringes are smooth and gradually change point-wise.

According to Eq. (5), there is no any black fringe appearing in the fringe field. Instead, such black fringes turn to white. Furthermore, the isochromatic fringe occurs when the fringe order $N = 0, \pm 1/2, \pm 3/2, \ldots$, which represents a half-fringed variation.

2.3 Determination of photoelastic parameters

To determine the photoelastic parameters, PST is used. There are several approaches available depending on the numbers of phase steps. In this paper, four-stepped PST is considered.

2.3.1 Isoclinic parameter

By applying the four-stepped PST to Eq. (4) according to the relation $\beta = (m - 1)\pi/8$, four intensity equations are given. Note that m refer to the phase step number ($m = 1, 2, 3, 4$). These equations are, then, mathematically combined to get the expression of isoclinic parameter as (Pinit and Umezaki, 2007)

$$\phi = \frac{\pi}{8} - \frac{1}{4} \arctan\left(\frac{I_1^s - I_3^s}{I_2^s - I_4^s}\right) \quad \text{for} \quad I_{\text{mod}}^s \neq 0 \quad (6)$$

where

$$I_{\text{mod}} = I_p \sin^2(\pi N) \quad (7)$$

$$I_m^s = I_{m,R} + I_{m,G} + I_{m,B} \quad (8)$$

$$I_{\text{mod}}^s = \sqrt{(I_1^s - I_3^s)^2 + (I_2^s - I_4^s)^2} \quad (9)$$

in Eqs. (8) and (9), the superscript 's' denote the summation over three wavelengths (R, G, and B) and the subscript 'mod' refers to the modulated intensity. It should be further noted that the isoclinic angles obtained using Eq. (6) lie in the range of 0 to $+\pi/4$ with modulo $\pi/4$.

2.3.2 Isochromatic parameter

Also applying the four-stepped PST to Eq. (5), four intensity equations are provided. By combining the third equation (third intensity map of stress field) with those previous four equations yields the expression for determination

of isochromatic parameter as following (Pinit and Umezaki, 2008)

$$N^{\mathrm{r}} = \frac{1}{2\pi}\arccos\left(1-\frac{2I_{\mathrm{mod}}}{I_{\mathrm{p}}}\right) \quad \text{for} \quad I_{\mathrm{mod}} \le I_{\mathrm{p}}. \qquad (10)$$

The superscript 'r' denotes the relative fringe order in the range of 0 to 0.5. Note that there are three maps of N^{r} according to the three wavelengths R, G, and B. Since the cosine function (also inverse cosine function) is of even function, the map of the relative fringe order contains no abrupt phase jumps unlike the map of isoclinics (Eq. (6)) which contains abrupt phase jumps due to the use of inverse tangent function.

2.4 Unwrapping of photoelastic parameters

The problem of wrapped phase maps occurs because the physical ranges of the isoclinic parameter and isochromatic parameter are of $-\pi/2$ to $+\pi/2$ and 0 to $+\infty$, respectively. As seen in Eqs. (6) and (10), the isoclinic parameter and isochromatic parameter respectively lie only in the ranges of 0 to $+\pi/4$ and 0 to 1/2. The phase unwrapping is, therefore, required to bring the values of both parameters to their physical ranges.

The isoclinic and isochromatic unwrapping algorithms used here are those published elsewhere (Pinit and Umezaki, 2007 and 2008). The general principle of phase unwrapping can be found in the book of Ghiglia and Pritt (1998).

3. Simulation of photoelastic fringes

To confirm the performance of newly developed methods for solving the photoelastic parameters, such methods have to be tested with some simulated photoelastic fringes generated on the basis of the theory of elasticity. In this paper, a circular disk model under diametral compression is treated as an example since its stress components are exactly known.

The procedure of simulation is as follows (Pichet *et al*, 2008);

1) Define the stress components σ_{xx}, σ_{yy}, and τ_{xy}. Note that other coordinate system can be used, i.e., r-θ coordinate system. According to the theory of elasticity, the stress components are expressed as (Ramesh, 2000)

$$\begin{Bmatrix}\sigma_{xx}\\ \sigma_{yy}\\ \tau_{xy}\end{Bmatrix} = -\frac{2P}{\pi t}\begin{Bmatrix}\dfrac{(R-y)x^2}{r_1^4}+\dfrac{(R+y)x^2}{r_2^4}-\dfrac{1}{D}\\ \dfrac{(R-y)^3}{r_1^4}+\dfrac{(R+y)^3}{r_2^4}-\dfrac{1}{D}\\ \dfrac{(R+y)^2x}{r_2^4}-\dfrac{(R-y)^2x}{r_1^4}\end{Bmatrix} \qquad (11)$$

where $r_1^2 = x^2+(R-y)^2$, $r_2^2 = x^2+(R+y)^2$, D and R are the diameter and radius of the disk, respectively. The origin of the coordinate system (x-y) is at the disk's center.

2) Determine the fringe order using the equation below for each wavelength

$$N = \frac{t}{f_\sigma}\{(\sigma_{xx}-\sigma_{yy})^2+4\tau_{xy}^2\}^{1/2} \qquad (12)$$

3) Determine the isoclinic angle using

$$\phi = \frac{1}{2}\arctan\left(\frac{2\tau_{xy}}{\sigma_{xx}-\sigma_{yy}}\right). \qquad (13)$$

It is seen that Eq. (13) provides ϕ in the range of $-\pi/4$ to $+\pi/4$ with modulo $\pi/2$. However, this range can be easily change to the range of 0 to $+\pi/2$ by adding $+\pi/4$ to all of isoclinic values.

4) Substitute the fringe order N and the isoclinic angle ϕ into Eqs. (4) or (5) by setting $I_{\mathrm{p}} = 255$ and $I_{\mathrm{b}} = 0$.

4. Implementation

The software is implemented in VC++ as stand-alone software. It can be installed on any computer and can analyze photoelastic parameters upon providing the photoelastic fringe images. The software has four main modules: data simulation, data reduction module, data visualizing module, and image processing module. The data simulation is for the generation of photoelastic fringes. The simulated fringes are used to test any new developed technique for solving the photoelastic parameters. The data reduction module contains a computational code, a phase unwrapping code for photoelastic parameters. The data visualizing module is to convert the data from the first module to forms that are easy to interpret by the user. The patterns of visualization can be either gray scale or color scale depending on the user. Further, there are several functions providing the quantitative and qualitative comparison. The last module - image processing module - provides some image processing functions such as noise removal function, image plane splitter, low pass and high pass filters, etc. This module helps user for both preprocessing and post processing.

Figures 3 and 4 show the main window of the developed program. Figure 3 displays the simulated photoelastic fringe whereas Figure 4 shows the input dialog for the generation of the opened image shown in Figure 3.

5. Results

5.1 Geometry of circular disk model and load condition

For simulation, the circular disk model with 30 mm in diameter and 6 mm in thickness is used. Its material stress fringe values (f_σ) for three RGB wavelengths are, respectively, f_σ,R = 11.19, f_σ,G = 10.01, and f_σ,B = 7.997 N/ (mm·fringe). These three material fringe values are used in Eq. (12). Further, the applied load P has a value of 274 N.

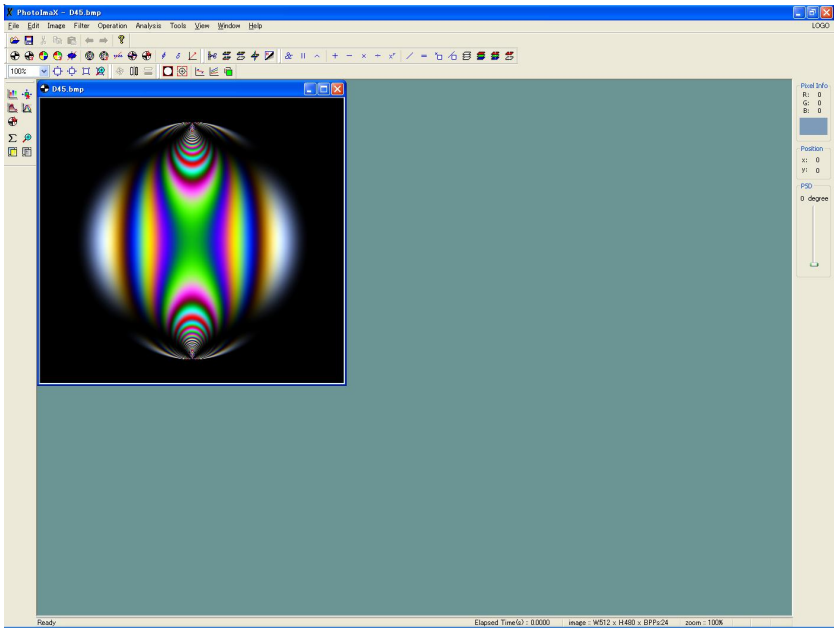

Figure 3. Main window of program after executing and opening an image. This image is printed in black and white.

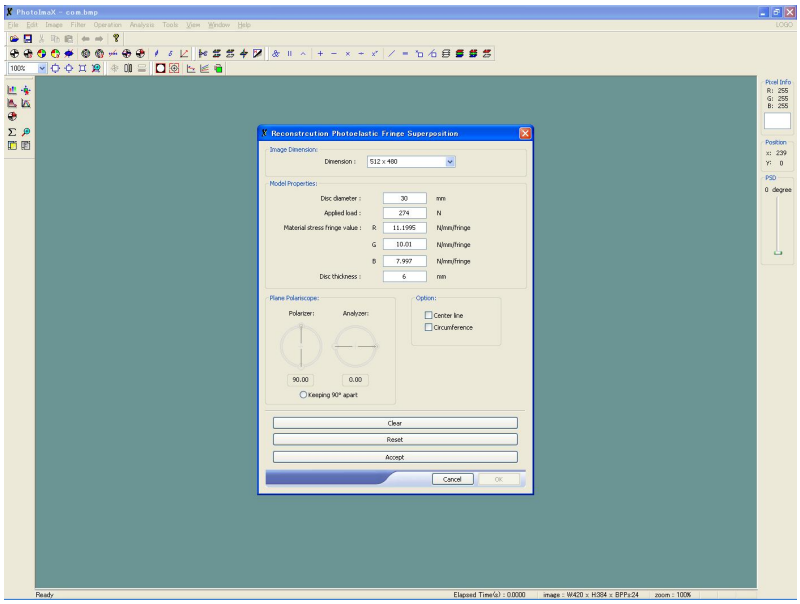

Figure 4. Input dialog to generate the fringe image shown in Figure 3. This image is printed in black and white.

5.2 Graphical plotting for data visualization

For data visualization, the values of isoclinics are converted to the gray map using the following equation.

$$g(x,y) = \mathrm{INT}\left[255\left(\frac{\phi - \phi_{\min}}{\phi_{\max} - \phi_{\min}}\right)\right] \quad (14)$$

and for isochromatic parameter, the gray map can be obtained using

$$g(x,y) = \mathrm{INT}\left[255\left(\frac{N}{N_{\max}}\right)\right]. \quad (15)$$

In Eqs. (14) and (15), g(x, y) is the gray level value of the pixel at the position (x, y) and INT[] gives the nearest integer. $\phi_{\max}$ and $\phi_{\min}$ are the maximum and minimum values of isoclinics in the range considered and $N_{\max}$ is the predefined maximum fringe order which can take any value being greater than unity.

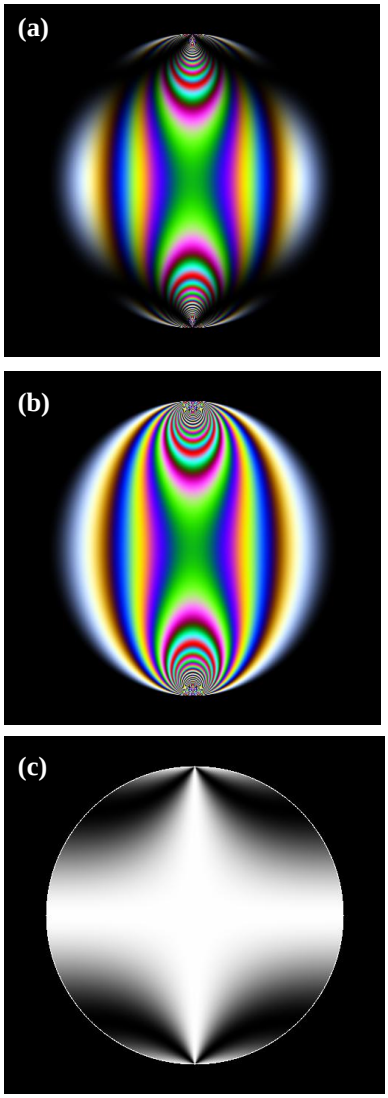

Figure 5. Color dark-field fringe pattern of the circular disk model under diametral compression: (a) photoelastic fringe, (b) isochromatic fringe, and (c) isoclinic fringe. These fringes are printed in black and white.

5.3 Simulated and numerical results

5.3.1 Photoelastic fringe

Figure 5a shows the photoelastic fringe of the disk model generated using the procedure described in section 3. The fringe contains both isochromatic (Figure 5b) and isoclinic (Figure 5c) fringes. The isochromatic fringe was obtained from Eq. (4) without the term $\sin^2 2(\phi - \beta)$ whereas the isoclinic fringe was also given by Eq. (4) without the term $\sin^2(2N)$.

5.3.2 Isoclinic map

Using Eqs. (11), (13), and (14) yields the isoclinic map in the range of $-\pi/4$ to $+\pi/4$. Figure 6a reports such map. Note

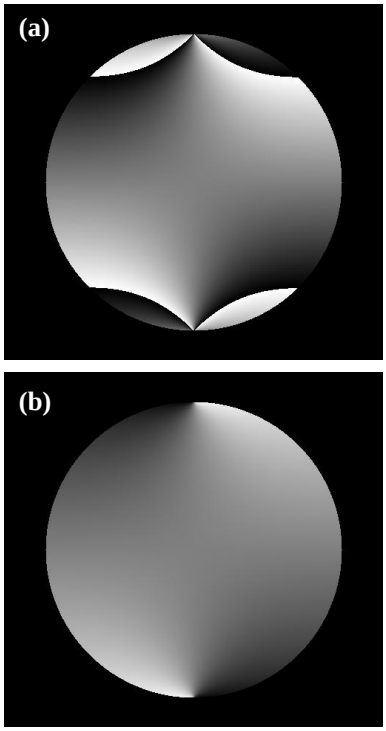

Figure 6. Isoclinic maps expressed in the ranges of (a) $-\pi/4$ to $+\pi/4$ and (b) $-\pi/2$ to $+\pi/2$.

that Eq. (13) can be found in the subject of Mechanics of Materials. However, for this problem, the equation for determination of isoclinic parameter is also expressed as (Frocht, 1948)

$$\phi = \arctan\left(\frac{2xy}{R^2 + x^2 - y^2}\right) \tag{16}$$

where the parameters in Eq. (16) are the same as those mentioned in section 3.

By Eq. (16), the isoclinic values in the range of $-\pi/2$ to $+\pi/2$ can be simply obtained and Figure 6b show the map in this range. It should be noted that Eq. (16) results from the Theory of Elasticity. In photoelasticity, one cannot get the map in the range of $-\pi/2$ to $+\pi/2$ directly but has to use the phase unwrapping (see section 2.4). Applying the phase unwrapping (Pichet and Umezaki, 2007) to the map in the range of $-\pi/4$ to $+\pi/4$ yields the same map in the range of $-\pi/2$ to $+\pi/2$ as shown in Figure 6b.

5.3.3 Isochromatic map

Applying Eqs. (12) and (15) yield the isochromatic map in the range of 0 to 20 fringe orders. Figure 7a displays such isochromatic map in the spectrum color of visible light and this shows the color map plotting in data visualization which is convenient. Note that Eq. (12) can provide $0 \le N \le N_{max} \approx +\infty$. As a result, the larger is the value of N_{max}, the smaller is the (red) circle appearing at the top and bottom of the disk.

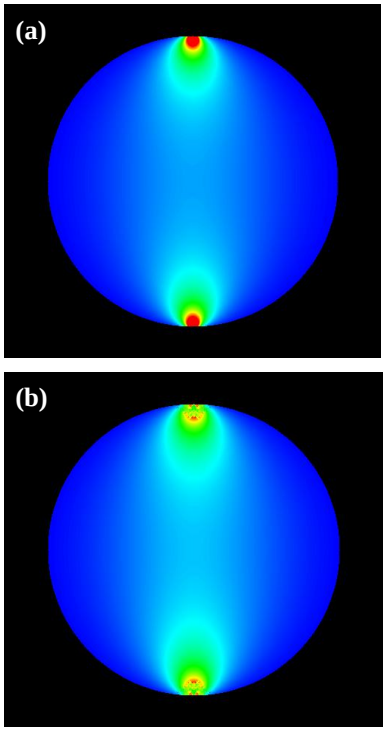

Figure 7. Isochromatic maps for (a) 0 to 20 and (b) 0 to 12 fringe orders. The maps were finally converted into spectrum color of visible light for the sake of clarity where the blue represents 0 and the deep red represents N_{max}. Note that the conversion is non-linear. These maps are printed in black and white.

Figure 7b reports the isochromatic map shown in the same spectrum color; however, the map was obtained from the phase unwrapping (Pichet and Umezaki, 2008); that is, the relative map of isochromatics N^{r} (Figure 5b) was given from Eq. (10) where $0 \leq N^{r} \leq 0.5$ and it was directly put into the phase unwrapping program. Note that the maximum value of N obtained is approximately of 12 fringe orders. The unreliable pixels at the top and bottom parts results from the high fringe density due to the application of the loads. These locations technically limit the value of N_{max} and this is the great issue in the field of digital photoelasticity.

6. Conclusion

The Windows-based software is developed as a helping tool for two-dimensional stress analysis and data visualization. The main technique based on the digital photoelasticity used in the code is the phase stepping technique. Two phase unwrapping algorithms for isoclinic and isochromatic unwrapping methods are implemented. The results obtained on the basis of the digital photoelasticity agree well with those obtained from the Theory of Elasticity and they express the validity of such algorithms. As a first step, the software developed can be used as an educational aid. Other models having the exact solution of the stress components can be easily simulated using the procedure mentioned in section 3. This is useful in teaching of digital photoelasticity and in validating any newly developed approach for analysis of photoelastic parameters.

In order to make the software more practicable for solving the engineering design or the industrial problems, the following aspects are considered;

1. Since, by principle, the isochromatic parameter pertains to the stress field of $(\sigma_1 - \sigma_2)$, the separation is needed such that the stress components σ_{xx}, σ_{yy}, and τ_{xy} or the individual σ_1 and σ_2 are retrieved. These stress components are subsequently used in the theories of failure for designing of the structural members in question. The process of separation requires unwrapped isoclinic and isochromatic data, which are readily obtained from the program. Although several researchers have proposed the separation techniques (Ramesh, 2000), these techniques only were just applied to the benchmark problem (see Eq. (11)) and they would fail when being applied to complicated models such as a model having discontinuities in the fringe field. The stress separation for complicated models should be, therefore, addressed in the future.

2. Digital photoelasticity needs the plastic model such that the fringe can be viewed; therefore, performing the real experiment may take time due to the preparation of the models. With the new technology of rapid prototyping (RP), construction of those models is then no longer tedious (Curtis *et al.*, 2003, Karalekas and Agelopoulos, 2004) in that the complicated models can be simply manufactured. Applying the software to the fringe images of such models built from the RP technology could make the fringe analysis faster. This could be beneficial for engineering design.

References

Curtis, J.D., Hanna, S.D., Patterson, E.A., and Taroni, M. 2003. On the use of stereolithography for the manufacture of photoelastic models. Experimental Mechanics, 43, 148-162.

Chen, T.Y.-F. 1999. Selected paper on photoelasticity. SPIE Optical Engineering Press, Washington.

Chen, T.Y., Hou, P.H. and Chiu, J.Y. 2002. Measurement of the ball screw contact angle by using the photoelastic effect and image processing. Optics and Laser in Engineering, 38, 87-95.

Frocht, M.M. 1948. Photoelasticity, Vol. 2, John Willey and Sons, New York.

Ghiglia, D.C. and Pritt, M.D. 1998. Two-dimensional Phase Unwrapping: Theory, Algorithms and Software, Wiley-Interscience, U.S.A.

Jeamic′, B., Scheuermann, G., Frey, J., Yang, Z., Hamann, B., Joy, K.I., and Hagen, H. 2002. Tensor visualizations in computational geomechanics. International Journal for Numerical and Analytical Methods in Geomechanics, 26, 925-944.

Jones, I.A. and Wang, P. 2005. An overdetermined phase-

stepping strategy for the capture of high-quality photoelastic data. Journal of Strain Analysis, 40, 477-492.

Jones, I.A., Truman, C.E. and Booker, J.D. 2008. Photoelastic investigation of slippage in shrink-fit assemblies. Experimental Mechanics, 48(5), 621-633.

Karalekas, D.E., Agelopoulos, A. 2004. On the use of stereolithography built photoelastic models for stress analysis investigations. Optics and Laser in Engineering, 27, 100-106.

Krishnaswamy, R. –C. 2005. Murray Lecture: Role of experiments in mechanics. Experimental Mechanics, 45, 478-492.

Patterson, E.A. and Wang, Z.F. 1991. Toward full field automated photoelastic analysis of complex components. Strain, 27, 49-56.

Patterson, E.A. 2002. Digital photoelasticity: principles, practice and potential. Strain, 38, 27-39.

Pindera, J.T. 2002. Patterns of modern experimental mechanics: principles of modeling of actual responses of materials, machines and structures. In Recent Advances in Experimental Mechanics, Gdoutos, E.E., editor. Kluwer Academic Publisher, the Netherland, pp. 571-584.

Pinit, P. and Umezaki, E. 2007. Digitally whole-field analysis of isoclinic parameter in photoelasticity by four-step color phase shifting technique. Optics and Laser in Engineering, 45, 795-807.

Pinit, P. and Umezaki, E. 2008. Absolute fringe order determination in digital photoelasticity. Journal of Solid Mechanics and Materials Engineering, 2, 519-529.

Pinit, P., Nuttawat, P. and Saranyu, M. 2008. A Simulation of fringe pattern of stress field for photoelasticity. Proceedings of the 6th PSU-Engineering Conference, Songkla, Thailand, May 8-9, 2008, pp. 659-664. [in Thai]

Ramesk, K. 2000. Digital Photoelasticity: Advanced Techniques and Applications, Springer, Berlin.

Spitas, V.A., Costopoulos, T.N. and Spitas, C.A. 2006. Optimum gear tooth geometry for minimum fillet stress using BEM and experimental verification with photoelasticity. Journal of Machine Design, 128, 1159-1164.

Wang, M.-J. 2003. A new photoelastic investigation of the dynamic bending stress of spur gears. Journal of Machine Design, 125, 365-372.

Wunsche, B. 1999. The visualization of 3D stress and strain tensor fields. Proceedings of the 3rd New Zealand Computer Science Research Student Conference, University of Waikato, Hamilton, New Zealand, Apirl 1999, pp. 109-116.

Zheng, Y., Lewis, R.W., and Gethin, D.T. 1995. FEView: An interactive visualization tool for finite elements. Finite Element in Analysis and Design, 19, 261-294.

Zuccarello, B. and Ferrante, S. 2005. Use of automated photoelasticity to determine stress intensity factors of bimaterial joints. Journal of Strain Analysis, 40, 785-800.